PNAS RESEARCH ARTICLE | MICROBIOLOGY CHEMISTRY

Re-sensitization of *mcr* carrying multidrug resistant bacteria to colistin by silver

Qi Zhang[a,1], Runming Wang[a,1], Minji Wang[b], Chunjiao Liu[c], Mohamad Koohi-Moghadam[a,d], Haibo Wang[a], Pak-Leung Ho[c], Hongyan Li[a], and Hongzhe Sun[a,2]

Edited by Robert Bonomo, Case Western Reserve University and Louis Stokes Cleveland VA, Cleveland, OH; received October 28, 2021; accepted February 1, 2022 by Editorial Board Member Richard P. Novick

Colistin is considered the last-line antimicrobial for the treatment of multidrug-resistant gram-negative bacterial infections. The emergence and spread of superbugs carrying the mobile colistin resistance gene (*mcr*) have become the most serious and urgent threat to healthcare. Here, we discover that silver (Ag^+), including silver nanoparticles, could restore colistin efficacy against *mcr*-positive bacteria. We show that Ag^+ inhibits the activity of the MCR-1 enzyme via substitution of Zn^{2+} in the active site. Unexpectedly, a tetra-silver center was found in the active-site pocket of MCR-1 as revealed by the X-ray structure of the Ag-bound MCR-1, resulting in the prevention of substrate binding. Moreover, Ag^+ effectively slows down the development of higher-level resistance and reduces mutation frequency. Importantly, the combined use of Ag^+ at a low concentration with colistin could relieve dermonecrotic lesions and reduce the bacterial load of mice infected with *mcr-1*–carrying pathogens. This study depicts a mechanism of Ag^+ inhibition of MCR enzymes and demonstrates the potentials of Ag^+ as broad-spectrum inhibitors for the treatment of *mcr*-positive bacterial infection in combination with colistin.

antimicrobial resistance | colistin | metalloenzymes | MCR-1 | silver

Significance

Superbugs carrying a mobile colistin resistance gene (*mcr*) are jeopardizing the clinical efficacy of the last-line antibiotic colistin. The development of MCR inhibitors is urgently required to cope with antibiotic-resistance emergencies. Here, we show that silver (Ag^+) fully restores the susceptibility of *mcr-1*–carrying superbugs against colistin both in vitro and in vivo. We found an unprecedented tetra-silver center in the active-site pocket of MCR-1 through the substitution of the essential Zn^{2+} ions in the intact enzyme, leading to the prevention of substrate binding (i.e. the dysfunction of MCR-1 in transferring phosphorylethanolamine to lipid A). Importantly, the ability of Ag^+ to suppress resistance evolution extends the lifespan of currently used antibiotics, providing a strategy to treat infections by *mcr*-positive bacteria.

The emergence and spread of multidrug-resistant (MDR) or extensively drug-resistant (XDR) gram-negative bacteria have renewed interest in the use of polymyxins (polymyxin B and colistin). Polymyxins are a class of cationic polypeptide antibiotics, which kill gram-negative pathogens through disruption of membrane permeability via polar and hydrophobic interactions. Despite having serious adverse effects, polymyxin B and colistin have become the last-resort treatment options for MDR and XDR bacterial infections (1, 2). Colistin resistance was predominantly caused by phosphoethanolamine (pEA) transferases, which catalyze the addition of phosphorylethanolamine (pEtN) to lipid A to reduce the electrostatic attraction between colistin and the gram-negative outer membrane (3–6). Such transmission has minimal clinical threats as it is chromosome mediated (2, 7, 8). However, the emergence and global spread of the first plasmid-borne transmissible colistin resistance gene, called mobile colistin resistance gene-1 (*mcr-1*), which was identified in 2015 (9), have significantly challenged the efficacy of this last-resort antibiotic. The MCR-1 enzyme encoded by the *mcr-1* gene, belonging to the alkaline phosphatase (AP) metalloenzyme superfamily based on its structure (10, 11), contains an essential Zn(II) cofactor in its active site coordinated with Glu^{246}, Asp^{465}, His^{466}, and phosphorylated Thr^{285} (TPO^{285}) (11–14). It catalyzes the addition of pEtN moiety from those such as phosphatidylethanolamine (PE) to lipid A of the gram-negative membrane as shown in *SI Appendix*, Fig. S1. In addition to the *mcr-1* gene, other families have also been identified, including *mcr-2*, *mcr-3*, *mcr-4*, and *mcr-5*, and each has its variants (1). These plasmid-borne resistances can be cross-spread rapidly via horizontal gene transfer between bacterial strains and species, resulting in the emergence of MDR superbugs (15, 16), which poses a significant challenge to clinicians.

Combination therapy comprising an available antibiotic and a nonantibiotic (as a resistance breaker) has been considered a safer, more economical and effective alternative than the development of new antibiotics (8, 17, 18). Such therapies have been successfully utilized clinically to treat infections caused by superbugs carrying serine-β-lactamases (SBLs) (19, 20). Metal-based agents have received increasing attention in coping with the current crisis of antimicrobial resistance (21–23). As resistance breakers, metal compounds have many advantages over organic compounds (24–26), in particular in the case that resistance is caused by a metalloenzyme such as metallo-β-lactams (MBLs), because metal ions can readily substitute the cofactors of metalloenzymes (8), resulting in broad-spectrum bactericidal activity (27, 28). Indeed, bismuth drugs such as colloidal bismuth subcitrate (CBS;

Author contributions: P.-L.H. and H.S. designed research; Q.Z., R.W., M.W., C.L., M.K.-M., and H.W. performed research; and H.L. wrote the paper.

Competing interest statement: H.S., P.-L.H., Q.Z., R.W., and H.L. have filed a patent application (US Provisional Application No. 62/890,667) related to the work of this manuscript.

This article is a PNAS Direct Submission. R.B. is a guest editor invited by the Editorial Board.

[1]Q.Z. and R.W. contributed equally to this work.

[2]To whom correspondence may be addressed. Email: hsun@hku.hk.

This article contains supporting information online at http://www.pnas.org/lookup/suppl/doi:10.1073/pnas.2119417119/-/DCSupplemental.

Published March 9, 2022.

De-Nol) have been recently shown to serve as broad-spectrum MBL inhibitors to treat MBL-positive bacterial infections in combination with antibiotics (8). The use of colistin in combination with other antibiotics (e.g., rifampin) (4, 6, 19) to treat MCR-1–producing bacterial infections may result in the emergence of multiresistant bacterial strains.

Here, we screened a panel of compounds and found that silver (Ag^+) could restore colistin efficacy against bacteria carrying the *mcr-1* gene and that its variants also effectively suppressed their evolution. Importantly, the combined use of colistin and silver nitrate ($AgNO_3$) at a low concentration could boost the in vivo efficacy of colistin in both murine peritonitis infection and wound infection models. Biophysical studies show that Ag^+ inhibits the MCR-1 enzyme through irreversible substitution of Zn^{2+}. Further X-ray crystallographic studies reveal that silver binds at the active site, and unexpectedly, a tetra-nuclear silver(I) center was formed in the active-site pocket of the enzyme, prohibiting the substrate binding. This study clearly unveils atomic details on Ag^+ inhibition of the MCR-1 enzyme and also highlights the potential of silver, including silver nanoparticles, to combat antimicrobial resistance.

Results and Discussion

Silver Restores Colistin Activity against *mcr*-Positive Bacteria In Vitro. By using Luria-Bertani (LB) broth, a nutritionally rich medium primarily used for the growth of bacteria, a panel of compounds, including 2 Zn^{2+} chelating agents, 4 bioligands, and 16 metal-based compounds, were initially screened against *mcr-1*–positive *Escherichia coli* (*E. coli* J53, denoted as MCR-1–J53 hereafter), which was confirmed to be resistant to colistin as judged by a minimal concentration to inhibit the 90% bacterial growth (MIC) of 8 μg mL^{-1} (6.93 μM) (9, 29). The growth inhibition was examined in the presence of compounds at a fixed concentration (1 μg mL^{-1}) and colistin at a subinhibitory concentration (1 μg mL^{-1}) (0.87 μM) for 16 h after bacterial inoculation. Primary screening results (*SI Appendix*, Fig. S2 and Table S1) showed that $AgNO_3$ exhibited the highest activity with over 90% growth inhibition being observed based on optical density (OD_{600}) reading.

Despite Ag^+ exhibiting wide-spectrum antimicrobial activity through targeting multiple biological pathways via inactivation of key enzymes (27), there appears no report that Ag^+ might serve as a resistant breaker rather than an antimicrobial agent. We first examined whether $AgNO_3$ could resensitize MCR-1 producers toward colistin. The standard checkerboard microdilution method (8, 30, 31) was used to monitor the interaction between colistin and $AgNO_3$ against MCR-1–J53 (Fig. 1*A*). A *mcr-1*–negative J53 strain with MICs of 0.5 μg mL^{-1} (0.43 μM) for colistin and 4 μg mL^{-1} (23.69 μM) for $AgNO_3$ individually (*SI Appendix*, Fig. S3) served as the negative control. $AgNO_3$ itself at the concentration of 1 μg mL^{-1} (5.92 μM) showed no or minor growth inhibition toward either *mcr-1*–positive (Fig. 1*A*) or -negative bacteria (*SI Appendix*, Fig. S3). However, when $AgNO_3$ and colistin were used in combination, $AgNO_3$ at a concentration as low as ca. 0.5 to 1.0 μg mL^{-1} (2.96 to 5.92 μM) could resensitize *mcr-1*–positive bacterium to colistin with the MIC value of colistin dropped by 16-fold from 8 μg mL^{-1} (6.93 μM) to 0.5 μg mL^{-1} (0.43 μM) (Fig. 1*A*), which is susceptible according to European Committee on Antimicrobial Susceptibility Testing (EUCAST) (the MIC breakpoint of colistin for a resistant isolate is >2 μg ml^{-1} (> 1.73 μM) (29). The fractional inhibitory concentration index (19) (FICI) was determined to be 0.375 (*SI Appendix*, Fig. S4*A*), indicative of the synergistic interaction between them (FICI of ≤0.5 is defined as synergism). In contrast, no such synergism was observed in *E. coli* J53 carrying no *mcr-1* gene (FICI of 0.625; *SI Appendix*, Fig. S4*A*), suggesting that, at a concentration of silver used, such a synergism is attributable to inhibition of MCR-1 by Ag^+. Time-kill curves further showed the time-dependent bactericidal effects of the drug combination against MCR-1–J53 and that the bacterial populations were lowered by over 10^5-fold after 24-h exposure to the combination of colistin (6 μg mL^{-1}, i.e., 5.19 μM) and $AgNO_3$ (2 μg mL^{-1}, i.e., 11.84 μM) in comparison to those in untreated or single-component groups (Fig. 1*B*).

In addition, the synergism between colistin and $AgNO_3$ was further observed in other *mcr-1*–carrying bacteria, including clinically isolated *Salmonella typhimurium 0839*, *Klebsiella aerogenes 7014*, *Klebsiella. pneumoniae 9607*, *Enterobacter kobei 4113*, and engineering strain *E. coli* BL21(DE3), with FICI values ranging from 0.25 to 0.37 (Fig. 1*C*). However, only partial synergies (0.5 ≤ FICI ≤ 1 is defined as partial synergism) were observed in some other bacterial species (*SI Appendix*, Fig. S4*A*). Given that mobilized resistance to colistin is evolving rapidly, different families and variants of *mcr-1* have been identified (8, 32). We therefore evaluated whether the colistin and $AgNO_3$ combination therapy could exhibit broad-spectrum antimicrobial properties against bacteria carrying other *mcr* genes. We selected *E. coli* J53 carrying five *mcr-1* variants and six *mcr* family genes and examined their susceptibility to the colistin and $AgNO_3$ combination. We found that in the presence of 1 μg mL^{-1} $AgNO_3$ (0.25 MIC), at which concentration Ag^+ exhibits almost no antimicrobial activity, the MIC values of colistin was decreased by ca. 16-fold to a susceptible level of 0.5 μg mL^{-1} (0.43 μM) against the bacteria carrying almost all *mcr* genes except *mcr-3* and *mcr-4* (Fig. 1*D*). This is reasonable as both *mcr-3* and *mcr-4* have been demonstrated to function differently from *mcr-1* (33, 34). This implies that the combination exhibits broad-spectrum antimicrobial activity against *mcr*-positive bacteria. A synergy was also observed when combined with silver nanoparticles (the size of 10 nm) under identical conditions (*SI Appendix*, Fig. S4*B*).

Silver Inactivates MCR-1 by Displacement of the Zn^{2+} Cofactor. MCR-1 catalyzes the addition of pEA to lipid A in the cell membrane to enhance the membrane potential of gram-negative bacteria (7, 35, 36). We first examined whether $AgNO_3$ was able to affect membrane potential owing to inhibition of MCR-1 activity in live cells using a membrane potential assay kit according to a standard protocol (37–39). The green/red fluorescence ratios, which are inversely correlated to membrane potential, were reduced by ca. 30% in *mcr-1*–positive *Shigella flexneri* compared with the negative control. Treatment of *mcr-1*–positive *S. flexneri* with $AgNO_3$ at 2 μg mL^{-1} (12 μM) led to the recovery of the fluorescence ratio to the levels found for the negative control (from 4.1 ± 0.4 to 5.8 ± 0.3). Consistent with this, supplementation of carbonyl cyanide chlorophenylhydrazone (CCCP; 5 μM), a potent mitochondrial uncoupling agent to dissipate the transmembrane potential (38), to *mcr-1*–positive *S. flexneri* led to an increase in the fluorescence ratio (green/red) to comparable levels (6.1 ± 0.1; Fig. 1*E*), indicating the recovery of membrane potential is attributable to inhibition of MCR-1 by $AgNO_3$. The inhibition was further confirmed on full-length MCR-1 by a thin layer chromatography (TLC) plate assay (35). The full-length MCR-1 (40 μM) was pretreated with or without 10 molar equivalents of $AgNO_3$ and mixed with a fluorescent substrate, NBD-

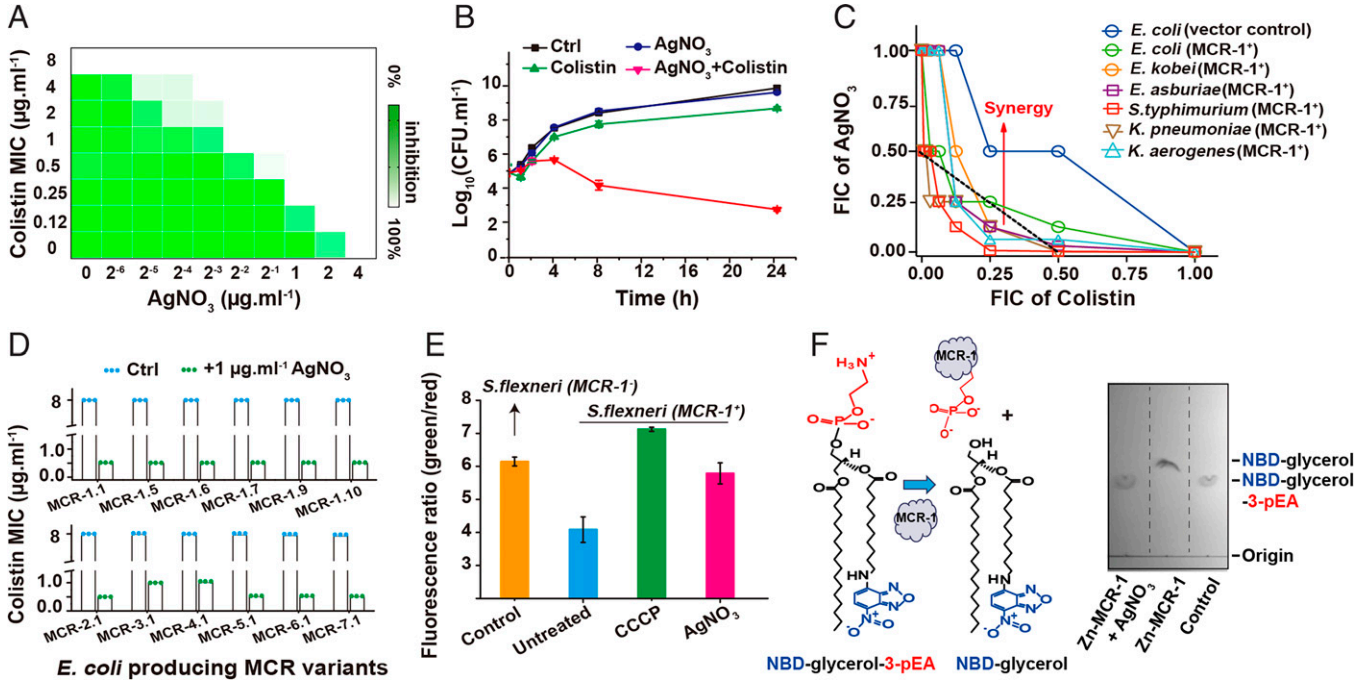

Fig. 1. $AgNO_3$ overcomes MCR(s)-mediated resistance by inhibiting enzyme activity. (*A*) Representative heat plots of microdilution checkerboard assay for the combination of colistin and $AgNO_3$ against MCR-1–J53. (*B*) Time-kill curves for colistin and $AgNO_3$ monotherapy or combination therapy against MCR-1–J53 during a 24-h incubation. The concentrations of compounds used in this test are $AgNO_3$ (2 μg mL^{-1}, 11.84 μM) and colistin (6 μg mL^{-1}, 5.19 μM). (*C*) Isobolograms of the combination of colistin and $AgNO_3$ against different *mcr-1*–positive bacterial strains. The black dashed line indicates an ideal isobole, where drugs act additively or independently. Data points below this line indicate synergism. (*D*) Bar charts showing the reduction of colistin MIC against *E. coli J53* carrying *mcr* variants when used in combination with $AgNO_3$ (1 μg mL^{-1}, 5.92 μM). Each test was performed in triplicate, and all values were showed as dots in the scatter-column diagram. (*E*) The membrane potential changes of *mcr-1*–positive and –negative *S. flexneri* upon $AgNO_3$ treatment as determined by the ratios of green to red fluorescent signals. Mean values of three replicates are shown and error bars indicate SD. *P* values were determined by Student *t* test. *P* values reflecting significance are below 0.001 (untreated/CCCP) and 0.002 (untreated/$AgNO_3$), respectively. (*F*) Inhibition of MCR-1 cleavage assay on NBD-glycerol-3-pEA by $AgNO_3$. The cleavage model for the chemical reaction catalyzed by MCR-1 (left) and the representative image of TLC plate (right) are shown here.

glycerol-3-pEA (1-palmitoyl-2-{12-[(7-nitro-2-1,3-benzoxadiazol-4-yl)amino]dodecanoyl}-sn-glycero-3-phosphoethanolamine) (Avanti Lipids), prior to the TLC-based detection. In contrast to native MCR-1, which cleaved pEA group from NBD-glycerol-3-pEA, resulting in the faster migration of NBD-glycerol, neither the $AgNO_3$ treatment group nor the substrate control group exhibited observable migration (Fig. 1*F*), which is indicative of the inhibition of cleavage activity of MCR-1 by $AgNO_3$.

As a soft metal ion, Ag^+ has been known to have a higher affinity to soft bases, such as cysteine residues in proteins (40), although other residues, such as histidine, might serve as additionally coordinated residues (28, 40). However, there is no free cysteine in MCR-1 that could coordinate to Ag^+ (11–14). To investigate whether Ag^+ could bind to MCR-1, we firstly overexpressed and purified the soluble catalytic domain of MCR-1 by sodium dodecyl sulphate–polyacrylamide gel electrophoresis (SDS-PAGE) (*SI Appendix*, Fig. S5*A*) and investigated the interaction of $AgNO_3$ with MCR-1–S in vitro. The intact MCR-1–S, which binds to 3 molar equivalents of Zn^{2+} as confirmed by inductively coupled plasma mass spectrometry (ICP-MS) (*SI Appendix*, Fig. S5*B*), denoted as Zn_3–MCR-1–S, at 20 μM was mixed with 150 μM PAR (4-(2-pyridylazo) resorcinol) (41). $AgNO_3$ at different ratios ranging from 2.5 to 40 was titrated into the protein solution and incubated at room temperature for 16 h. We observed the appearance and increase in the intensities of absorbance at ca. 495 nm ($Zn(PAR)_2$), accompanied by the decrease in the intensities of absorbance at ca. 395 nm (PAR), indicating that Ag^+ binds to native Zn_3–MCR-1–S, resulting in the release of Zn^{2+} from the enzyme (*SI Appendix*, Fig. S6*A*).

We further monitored the Ag^+ binding to the enzyme and subsequent release of Zn^{2+} from Zn_3–MCR-1–S by ICP-MS. As shown in Fig. 2*A*, the addition of increasing amounts of $AgNO_3$ to Zn_3–MCR-1–S resulted in a gradual decrease in the stoichiometry of Zn^{2+} to MCR-1–S, accompanied by the increase in the binding stoichiometry of Ag^+ to MCR-1–S, and eventually all Zn^{2+} (ca. 3.0 molar equivalents) were displaced, with ca. 10.2 molar equivalents of Ag^+ bound. Supplementation of excess amounts of Zn^{2+} to Ag^+-bound MCR-1–S resulted in negligible changes in the amounts of metals bound to MCR-1–S (*SI Appendix*, Fig. S6*B*), indicative of irreversible Zn^{2+} release under the experimental conditions.

We next measured the binding affinity of Ag^+ to apo–MCR-1–S by isothermal titration calorimetry (ITC). The ITC data were fitted by a sequential-binding model, giving rise to an apparent dissociation constant (K_d) of 0.29 ± 0.09 μM and binding capacity (N) of 9.77 ± 0.43 (Fig. 2*B*). Such a high binding capacity of Ag^+ was also observed in our matrix-assisted laser desorption/ionization-time of flight mass spectrometry (MALDI-TOF-MS) assay on Ag–MCR-1–S, where up to 9 Ag^+ (*m/z* 39623.132) were clearly shown to bind into apo–MCR-1–S (*m/z* 38663.015) successfully in vitro (*SI Appendix*, Fig. S7*A*). Notably, for comparison, the apparent K_d of Zn^{2+} to apo–MCR-1–S was also determined similarly to be 2.45 ± 0.93 μM (N= 2.87 ± 0.12; *SI Appendix*, Fig. S7*B*), suggesting that Ag^+ binds the metalloenzyme around 10-fold stronger than Zn^{2+} on the whole.

By using a cellular thermal shift assay (CETSA), we subsequently examined whether $AgNO_3$ binds to the enzyme in cellulo. *E. coli* BL21(DE3) cells expressing MCR-1–S after treatment with $AgNO_3$ at 1 μg mL^{-1} (5.92 μM) for 16 h in LB medium were harvested and subjected to CETSA analysis according to a standard protocol (42–44). As shown in Fig. 2*C*,

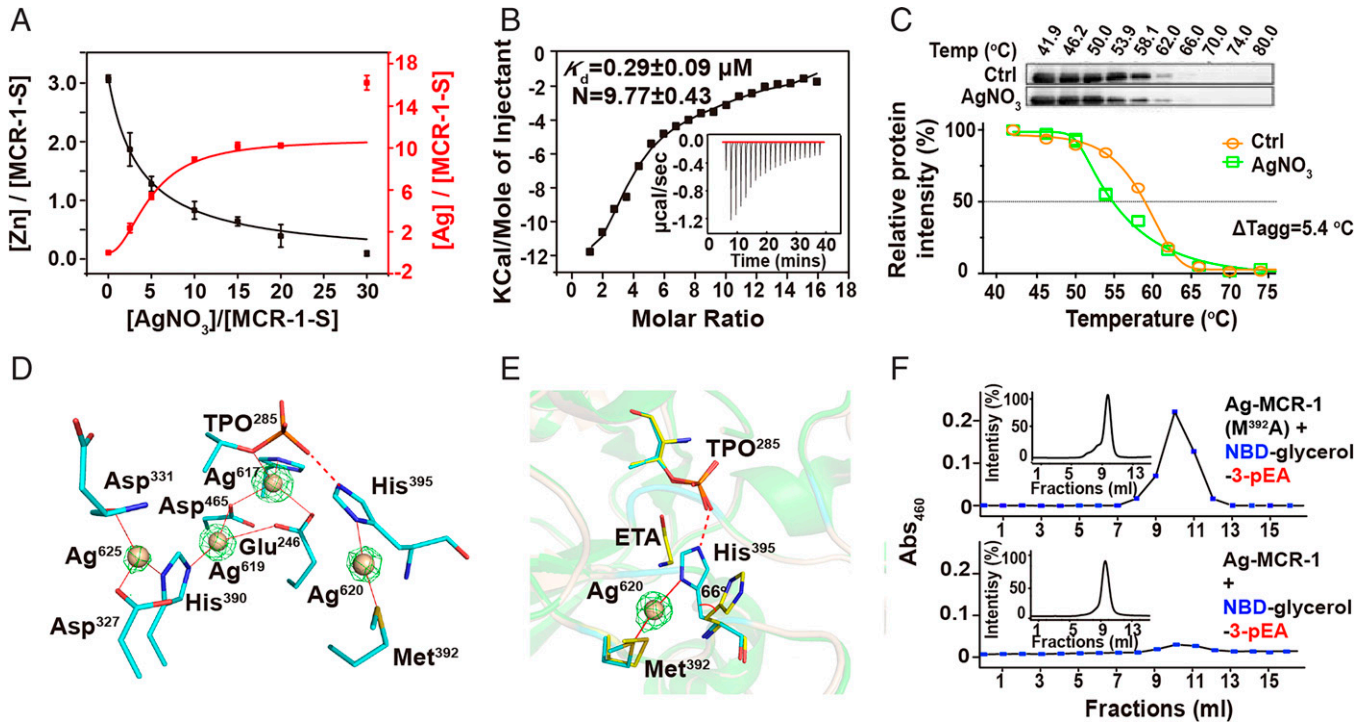

Fig. 2. Formation of a tetra-silver center releases cofactor Zn^{2+} from MCR-1–S and disrupts substrate binding. (*A*) The substitution of Zn^{2+} in MCR-1–S by $AgNO_3$ by equilibrium dialysis. (*B*) Representative ITC assay showing binding of $AgNO_3$ to apo–MCR-1–S. (*C*) CETSAs showing the binding of Ag^+ to soluble domain of MCR-1 in intact MCR-1–S producing *E. coli* BL21 (DE3) cells. The blotting is representative of three independent experiments. Ctrl, control. (*D*) The cartoon of tetra-nuclear silver center in the active-site pocket of the MCR-1–S enzyme. Ag^+ shown as wheat spheres are bridged in a narrow pocket by either coordination bonds (red solid lines) or hydrogen bond (red dash line). (*E*) Superimposition of Ag-bound MCR-1–S (PDB ID: 7WAA) (cyan) onto substrate analog (ETA, shown as yellow stick)-bound MCR-1–S (PDB ID: 5YLE) (yellow). A 66° rotation of the imidazole ring of His^{395} is clearly seen, which leads to steric hindrance for substrate binding. (*F*) Inhibition of substrate binding assays on Ag-bound MCR-1 with or without the mutation at Met^{392} ($M_{392}A$). NBD-glycerol-3-pEA, which gives rise to a UV absorbance at 460 nm, was used for the assay. The insets show the normalized absorbance at 280 nm for related the Ag-bound MCR-1 enzyme. All structures are refined by phenix 1.15, and occupancies of related silver ions are 0.7 (Ag^{617}), 0.5 (Ag^{619}), 0.6 (Ag^{620}), and 0.4 (Ag^{625}), respectively. The anomalous density signals are shown as green mesh contoured at 10σ (Ag^{617}, Ag^{620}) or 5σ (Ag^{619}, Ag^{625}). (*A* and *C*) Mean value of three replicates are shown, and error bars indicate SD.

treatment of $AgNO_3$ yielded ca. 5.4 °C decreases in the melting temperature (T_{agg}) of MCR-1–S, suggesting the binding of Ag^+ to MCR-1–S in cellulo. To further demonstrate that Ag^+ binds to the full-length MCR-1 in cellulo, *E. coli* BL21(DE3) overexpressing full-length MCR-1 (42, 45, 46) was treated with $AgNO_3$ at 3 μg mL^{-1} (17.77 μM) for 16 h and then harvested. The cell lysates from freeze-thawing in liquid nitrogen were analyzed by SDS-PAGE/western blotting, and the band at molecular weight ~60 kDa corresponding to full-length MCR-1 was subjected to ICP-MS analysis (*SI Appendix*, Fig. S8*A*). After normalization of cell contents by bicinchoninic acid (BCA) assays on total protein concentration, the silver content in the MCR-1 band was increased by ≥70% from cells supplied with 0.5 mM isopropyl β-D-1-thiogalactopyranoside (IPTG), in comparison to those without the addition of IPTG (*SI Appendix*, Fig. S8*B*), verifying the binding of Ag^+ to full-length MCR-1 in cells.

Silver Binds to MCR-1 at an Atomic Resolution. We then investigated the inhibitory mode of action of Ag^+ toward MCR-1 enzymes by X-ray crystallography. Cocrystallization of Ag(I)-bound MCR-1 or MCR-1–S was not successful, and thus crystal soaking with $AgNO_3$ was used. The Zn-bound MCR-1–S (Zn–MCR-1–S) crystal structure was firstly resolved at 1.83 Å as a homodimer in an asymmetric unit (Protein Data Bank [PDB] access code: 6LI4). Only one Zn^{2+} was found in the active site of each chain (anomalous signals, ≥20σ), coordinating to Glu^{246}, Asp^{465}, His^{466}, and TPO^{285} with a distorted tetrahedral geometry (*SI Appendix*, Fig. S9 *A* and *B*). The apo-form MCR-1–S crystals were obtained after soaking the native MCR-1–S crystals in a pool of cryosolution supplemented with ethylenediaminetetraacetate (EDTA-Na_2), and its structure was solved at a resolution of 1.82 Å (*SI Appendix*, Fig. S9 *C* and *D*). The Ag^+-bound MCR-1–S crystal (Ag–MCR-1–S, diffracted to 1.58 Å) was finally obtained after soaking the apo–MCR-1–S crystals into cryoprotectant solutions containing 1 mM $AgNO_3$ for 5 min in darkness.

The presence of Ag^+ was evidenced by both the anomalous signals (≥20σ) and significantly positive peaks (≥20σ) in the *mFo-DFc* (difference Fourier) map. Occupancies of Ag^+ were refined based on their B factors. On the electron density maps, 10 Ag^+ ions were identified in 1 chain of each asymmetric unit, in consistence with ITC and ICP-MS measurements (*SI Appendix*, Fig. S10*A*). Superimposition of the structures of Ag-bound with Zn-bound or apo-form MCR-1–S showed negligible overall conformational changes with rmsds of 0.471 Å and 0.779 Å over all alpha carbon (C*a*), respectively (*SI Appendix*, Fig. S10). In the original Zn^{2+} site, an Ag^+ (Ag^{617} with occupancy of 0.7) was found to coordinate with Glu^{246}, Asp^{465}, His^{466}, and TPO^{285}, forming a distorted tetrahedral geometry (Fig. 2*D*). These bond lengths for Ag^+ were longer than those for Zn^{2+} in general, probably owing to the larger ionic radius of Ag^+ (1.15 Å) than Zn^{2+} (0.74 Å) (*SI Appendix*, Tables S2 and S3).

Besides, three additional Ag^+ ions with occupancies ranging from 0.4 to 0.6 were also observed with either linear (Ag^{620}) or trigonal (Ag^{619} and Ag^{625}) geometries (Fig. 2 *D* and *E*). Six subsidiary Ag^+ sites were located on the surface of MCR-1–S

with linear geometry, and one of them (Ag^{626}) was only observed in one chain in the asymmetric unit with occupancy of ca. 0.5 (*SI Appendix*, Fig. S11), implying less accessibility of Ag^+ to this site. Considering their coordination environments, there appeared a faint possibility that the six Ag^+ showed direct inhibitory effects on MCR-1. Except for Ag^{617}, all the other Ag^+ possessed different metal-binding sites (*SI Appendix*, Table S3) from those of Zn^{2+} based on previous reports (11–14). Their coordinating residues and corresponding bond lengths with the side chains are summarized in *SI Appendix*, Table S3. These crystallographic studies supported our biophysical data that Ag^+ inactivates the enzyme through the displacement of Zn^{2+} of MCR-1–S.

Certain critical residues served as the μ_2-bridging ligands to yield an unprecedented tetra-nuclear silver center in the active-site pocket of MCR-1 (47–50) (Fig. 2 *D* and *E* and *SI Appendix*, Fig. S12). Specifically, in addition to the active site Ag^+ (Ag^{617}), Ag^{619} was bridged with Ag^{617} via $O\delta_2$ of Asp^{465} and $O\varepsilon_1$ of Glu^{246} and further coordinated to $N\varepsilon_2$ of His^{390} with a trigonal geometry. The bond lengths of Ag^{619} to His^{390}-$N\varepsilon_2$, Asp^{465}-$O\delta_2$, and Glu^{246}-$O\varepsilon_1$ varied from 2.30 to 2.77 Å, with a quasi-linear His^{390}-$N\varepsilon_2$-Ag^{619}-Asp^{465}-$O\delta_2$ angle of 159.1° and planar His^{390}-$N\varepsilon_2$-Ag^{619}-Glu^{246}-$O\varepsilon_1$-Asp^{465}-$O\delta_2$ dihedral of 161.9°. Moreover, Ag^{625} was bridged with Ag^{619} via $N\varepsilon_1$ of His^{390} and further bound to $O\delta_2$ of Asp^{327} and O of Asp^{331} with a quasiplanar Ag^{625}-His^{390}-$N\delta_1$-$N\varepsilon_2$-Ag^{619} dihedral of 170.9° (Fig. 2*D*). Interestingly, another Ag^+ (Ag^{620}) was also observed nearby which coordinated to Met^{392}-Sδ and His^{395}-$N\delta_1$ by a linear geometry with a comparable bond length of 2.02 Å and a quasilinear S-Ag^{620}-N angle of 170.7° (Fig. 2*D*). Notably, a strong hydrogen bond was formed between $N\varepsilon_2$ of His^{395} and O3P of TPO^{285}, which was coordinated by Ag^{617}, with a bond length of 2.49 Å to stabilize the silver center (Fig. 2*D*). Such a unique tetra-silver center in the active-site pocket of the MCR-1 enzyme was observed (12, 22), which illustrated the diversities of silver coordination environments and geometries in these proteins.

Notably, the binding of Ag^{620} to Met^{392} and His^{395} induced ca. 66° rotation of the imidazole ring of His^{395} and the shortening of the distance between $N\delta_1$/His^{395} and C*a*/ethanolamine (ETA) from 3.94 to 1.32 Å in the substrate-binding site of MCR-1 (Fig. 2*E*), in comparison to the MCR-1 complex with substrate analog ETA (PDB code: 5YLE). This possibly led to the prohibition of substrate binding to MCR-1 due to steric effects. To further validate the hypothesis, we investigated whether Ag^+ interfered with the binding of substrate (as NBD-glycerol-3-pEA) in MCR-1 and the MCR-1–M^{392}A variant. Ag-bound MCR-1, as well as Ag-bound MCR-1–M^{392}A, was mixed with an equal molar equivalent of NBD-glycerol-3-pEA and subsequently subjected to size-exclusive chromatography analysis. The absorbance at 280 and 460 nm was monitored for the detection of protein and NBD-glycerol-3-pEA-bound protein, respectively. As shown in Fig. 2*F*, the absorbance was only observed at 280 nm for the fraction of Ag-bound MCR-1, confirming the absence of substrate binding. In contrast, the absorbance was evident at both 460 and 280 nm for the fraction of MCR-1–M^{392}A under identical conditions, indicating the binding of NBD-glycerol-3-pEA to this mutant protein due to the lack of Ag^{620} at Met^{392}.

Collectively, crystallographic and biophysical data substantially demonstrated that Ag^+ played dual roles in abolishing MCR-1 activity through replacing Zn^{2+} with Ag^+ in the catalytic site and exhibiting steric effects in the substrate-binding site.

Silver Suppresses Resistance Evolution in *E. coli*-Carrying *mcr-1*. Considering the rapid evolution of *mcr* genes (51, 52), we therefore used an index of mutation prevention concentration (MPC) (53) to evaluate the effect of Ag^+ on the evolution of *mcr* genes against MCR-1–J53 in the absence and presence of different concentrations of Ag^+ (as $AgNO_3$). We found that colistin alone could not kill high-level resistant mutants even in the presence of 8-fold MIC (MPC = 16-fold MIC; Fig. 3 *A* and *B*). In contrast, with the increase in Ag^+ concentrations, the number of mutant colonies declined significantly as shown in the heat map (Fig. 3*B*). The observed mutation frequency ranged from 1.4×10^{-5} to 5.2×10^{-7}. However, no such reduction in mutant colonies was noted for the *mcr-1*–negative strain (*SI Appendix*, Fig. S13). The MPC of colistin was lowered to twofold MIC against MCR-1–J53 when Ag^+ ($AgNO_3$) was used at fivefold MIC, i.e., 20 μg mL^{-1} (117.74 μM) (Fig. 3 *A* and *B*). In contrast, less mutation prevention was observed for $AgNO_3$ in an *mcr-1*–negative bacterial strain (*SI Appendix*, Fig. S13). Notably, the combination therapy significantly suppressed the evolution of high-level resistance over a period of 16 passages of MCR-1–J53 (Fig. 3*C*). Gene sequencing of the 16th passage of *mcr-1*–positive bacteria upon treatment of colistin alone or in combination with $AgNO_3$ showed that no appearance of mutations occurred (*SI Appendix*, Fig. S14). Instead, the high level of resistance of the *mcr-1*–positive bacterium is likely attributable to the hyperproduction of the MCR-1 protein as revealed by a Western blotting assay, which showed a significant reduction (over 60%) in the level of MCR-1 in the bacterium treated by the combination therapy (Fig. 3 *C*, *Insert*).

Silver Restores Colistin Efficacy In Vivo. To further evaluate the potential utility of combination therapy in vivo, we first assessed their abilities to kill bacteria in mice infected by *mcr-1*–positive bacteria. Balb/c mice were injected intraperitoneally (i.p.) with a sublethal dose (2×10^6 colony-forming units [CFU] per mouse) of *K. pneumoniae 9607*, a clinical isolate producing MCR-1, and subsequently treated with a single dose of i.p. administration of vehicle control, Ag^+ (as $AgNO_3$ at 1.5 mg kg^{-1}), and colistin (2 mg kg^{-1}), and their combination (four mice in each group). After 48 h, all the mice were sacrificed, and bacterial loads in livers and spleens, which were severely infected by *K. pneumoniae 9607* according to a pre-experiment, were examined by agar plating. In comparison to the bacterial load (at the level of 10^5 CFU mL^{-1} g^{-1}) in both liver and spleen of mice treated by either $AgNO_3$ or colistin monotherapy, a significant reduction by >20-fold in the CFUs was observed in the combination therapy (Fig. 3 *D* and *E* and *SI Appendix*, Table S4).

Considering the urgency of treatment of skin infection caused by colistin-resistant bacteria producing MCR-1 (54–57), we further evaluated the efficacy of the combination therapy in the treatment of skin wound infected with *mcr-1*–positive bacteria. Similarly, a dose (2×10^6 CFU per mouse) of log-phased *mcr-1*–positive *K. pneumoniae 9607* was applied to skin wounds of Balb/c mice under the treatment of full-thickness skin defect overlying the thoracic region. Then, all mice were administrated once daily with the monotherapy of vehicle control, colistin (2 mg kg^{-1}), and Ag^+ (as $AgNO_3$ at 1 mg kg^{-1}), or their combination. As shown in *SI Appendix*, Fig. S15, both $AgNO_3$ and colistin monotherapy at the concentration used have less protection in relieving the dermonecrotic lesions after 7 d postinfection. Surprisingly, the combination therapy significantly facilitated the infected mice to recover

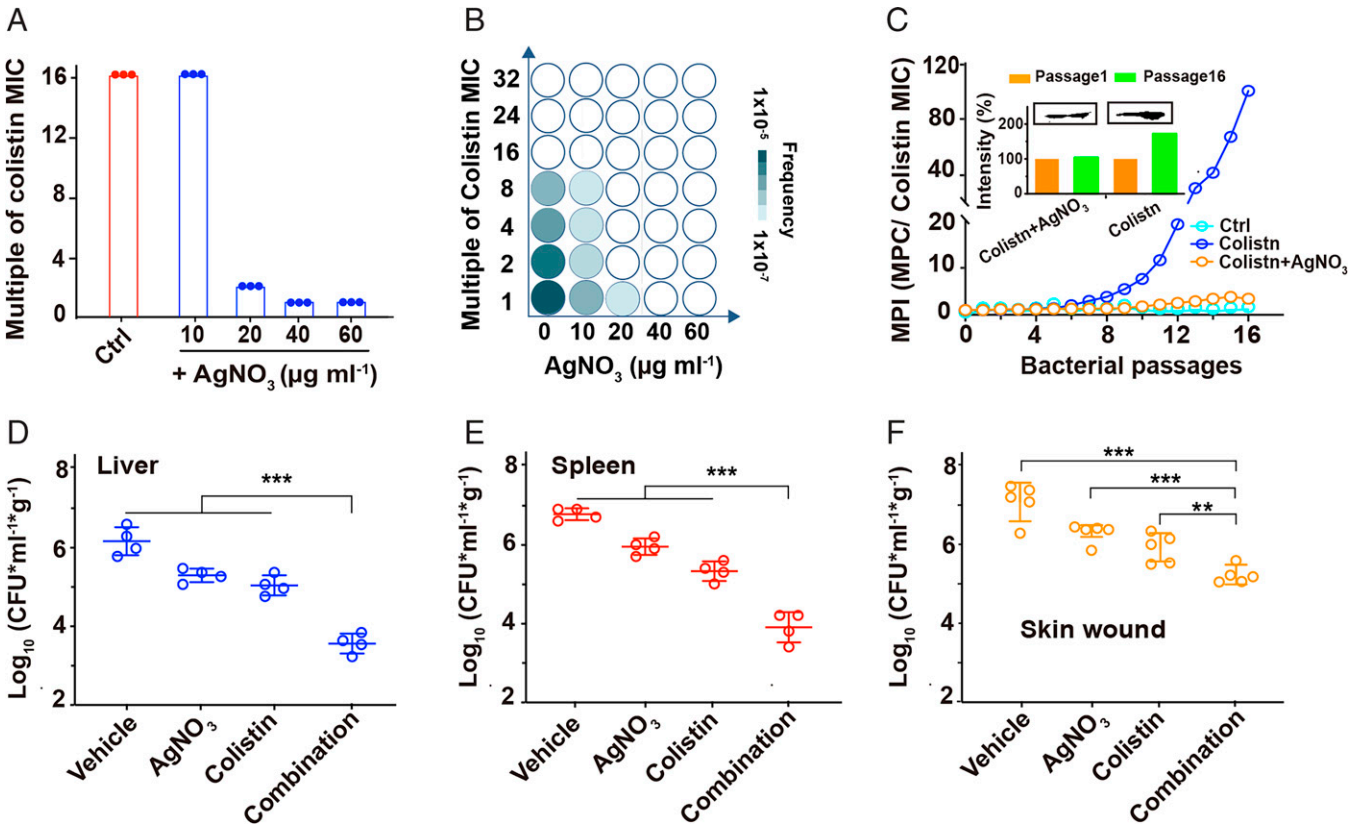

Fig. 3. The combination therapy of colistin and $AgNO_3$ suppresses the resistance development of MCR-1 and shows potency in vivo. (*A*) Vertical bar chart showing the MIC indices of colistin in the presence of increasing concentrations of $AgNO_3$ against MCR-1–J53. Each test was performed in triplicate, and all values were showed as dots in the scatter-column diagram. (*B*) Heat maps reflecting mutation frequencies of MCR-1–J53 exposed to colistin alone or combination of colistin and $AgNO_3$. (*C*) Resistance acquisition curves during 16 passages with the subinhibitory concentrations of colistin alone or a combination of colistin and $AgNO_3$ against MCR-1–J53. The inset shows the normalized expression level of MCR-1 in MCR-1–J53 receiving different treatments. (*D* and *E*) Bacterial loads in the liver (*D*) and spleen (*E*) of Balb/c mice infected with a sublethal dose of *K. pneumonia 9607* (MCR-1$^+$) and received single dose of i.p. administration of vehicle, monotherapy of $AgNO_3$ (1.5 mg kg^{-1}), and colistin (2 mg kg^{-1}), and their combination, respectively. (*F*) Bacterial loads in abscess area on day 7 in the wound infection model. Balb/c mice were infected with a sublethal dose of log-phased *mcr-1*–positive *K. pneumoniae 9607* and received a single dose of vehicle, monotherapy of colistin (2 mg kg^{-1}), or $AgNO_3$ (1 mg kg^{-1}), or their combination. (*D–F*) All *P* values were determined to reflect the significance difference from combination therapy group by Student *t* test. $^{**}P < 0.05$, $^{***}P < 0.001$.

from the wound infection, and the morphology lesions had been negligible (*SI Appendix*, Fig. S15). Similarly, the bacterial loads from wound beds were also significantly reduced by over 10-fold under the treatment of combination therapy in comparison with other treatments (Fig. 3*F*).

Silver is hardly used internally as an antimicrobial agent due to potential toxicity. Nevertheless, no apparent toxicity of silver at an administered dose of 6 mg kg^{-1} was observed in mice in a previous report (21). In this study, a much lower dose of silver (1.5 mg kg^{-1}) was used in combination with colistin, which already significantly reduced the bacterial load of *mcr-1*–positive bacteria in infected mice. This suggests that the toxicity of silver should not be a major concern if it is used as an adjuvant of antibiotics instead of antimicrobial agents. Collectively, we demonstrate that the in vitro antimicrobial efficacy of a combination therapy of $AgNO_3$ and colistin could be well translated into in vivo efficacy.

Conclusion

Our combined data show that $AgNO_3$ can restore the efficacy of colistin through binding and functional disruption of MCR enzymes. Importantly, the in vitro antimicrobial efficacy of combination therapy could be successfully translated into in vivo efficacy. X-ray crystallographic data clearly reveal a dual function of silver in the inhibition of MCR-1 activity via kick-off of Zn^{2+} as well as interference of the substrate binding. Such a phenomenon might be attributable to the unique features of Ag^+ coordination in proteins. Moreover, it should also be a complicated process which can be not only kinetically but also thermodynamically driven (40, 58), although it might be too rapid and tight to be accurately measured. The ability of silver as well as other metalloagents to inhibit key resistant determinants and to slow down the development of drug resistance (8, 42) offers a promising strategy for combating antimicrobial resistance when used in combination with antibiotics.

Materials and Methods

The construction of plasmids, gene mutations, compound screening, time-kill, drug resistance study, protein purification, membrane potential, enzyme activity, CETSA, ITC, MALDI-TOF, Zn^{2+} release analysis, mouse peritonitis, and wound infection models are described in the *SI Appendix*. All animal experiments were approved by and performed in accordance with the guidelines approved by Committee on the Use of Live Animals in Teaching and Research (CULATR) (Ref No.: 4008-16 and 5079-19), The University of Hong Kong.

X-Ray Crystallography. Zn^{2+}-bound MCR-1–S crystallization condition was screened using the sitting drop method by mixing equal volumes of protein and reservoir solution. The optimized reservoir solution contains 100 mM KSCN, 30 to 32% PEG 3350, and 100 mM Tris-HNO_3 (pH 8.0). The crystals appeared after

2 wk at 25 °C and were transferred into chelating buffer (32% PEG 3350, 100 mM Tris-HNO_3 [pH 8.0], 25% glycerol, and 10 mM EDTA-Na_2) for 12 h to prepare apo–MCR-1–S crystals. Next, these apo-crystals were washed three times in cryoprotectant solution (32% PEG 3350, 25% glycerol, and 100 mM Tri-HNO_3 [pH 7.5]) and then soaked in the buffer containing 1 mM $AgNO_3$, 32% PEG 3350, 25% glycerol, and 100 mM Tris-HNO_3 (pH 7.5) for different time lengths (from 1 min to 1 wk) in darkness. Then, the crystals were flash-frozen in liquid nitrogen. All data sets were collected using 0.979-Å synchrotron radiation at the BL17U1 beamline of Shanghai Synchrotron Radiation Facility (SSRF), Chinese Academy of Sciences (CAS). The diffraction data were processed with HKL2000 at SSRF. Molecular replacement was performed using the program Phaser suite, and Zn^{2+}-bound MCR-1 (PDB code: 5GRR) was used as the template model. The Ag^+ and Zn^{2+} occupancies were refined based on atomic B-factor. High Ag^+ occupancy ($\geq$0.7) and absorbance signal (σ, $\geq$20) prompted the success in the replacement of Zn^{2+}. Model rebuilding and refinement were performed by Refmac. TLS refinement was incorporated into late refinement stages. Solvents were added in Coot and refined by Refmac. The final models were validated with MolProbity. Details of the data collections and analysis and model refinement statistics are summarized in *SI Appendix*, Table S2.

Measurement of Metal Ions. Briefly, 10 μM apo–MCR-1–S was incubated with 100 μM $Zn(OAc)_2$ in dialysis buffer (50 mM Hepes [pH 7.4]) overnight at 4 °C to ensure that the metal ions were fully loaded onto these proteins. The unbound Zn^{2+} ions were removed by dialysis in a Zn^{2+}-free buffer to ensure that the metal ions were fully loaded into these proteins. The concentration of MCR-1–S with or without treatment were quantified by a BCA kit (Thermal Fisher Scientific), and metal contents were determined by ICP-MS (Agilent 7500a; Agilent Technologies) after digestion with 65% HNO_3 overnight using ^{115}In (5 ppb) as an internal standard. Considering the well-known similar chemical properties between Zn^{2+} and Co^{2+}, the molecular ratio of Zn^{2+} in MCR-1–S was double confirmed by a Co^{2+}-stimulation ICP-MS assay by using similar method. A similar protocol was also performed on full-length MCR-1 from *E. coli* BL21(DE3) by cutting and transferring the SDS-PAGE gel band into clear tubes with 65% HNO_3 to digest and analyze silver contents. ^{34}S contents were also measured for further quantification of protein concentration. These assays were performed in triplicate, and results were expressed as average ± SD.

Substrate Inhibition Assay. The substrate inhibition assay was performed by gel filtration and ultraviolet (UV) spectroscopy. Briefly, the apo-form of the full-length MCR-1 was incubated with 10 molar equivalents of $AgNO_3$ at 4 °C overnight. The resulting Ag-bound MCR-1 was incubated with equal molar NBD-glycerol-3-pEA in a substrate-reaction buffer (50 mM Hepes, 100 mM NaOAc, and 0.4% DDM [pH 7.5]) for 20 h and then applied into gel filtration in substrate-reaction buffer. A similar procedure was performed on apo–MCR-1 with an $M^{392}A$ mutation. All separated fractions were immediately subjected to UV-vis spectroscopy analysis in a range of 220 to 800 nm to record their intensities if present.

Data Availability. The coordinate and structure factor of Ag–MCR-1–S have been deposited in the PDB (accession code 7WAA). All other data are included in the article and/or *SI Appendix*.

ACKNOWLEDGMENTS. This work was supported by the Research Grants Council of Hong Kong (Fund number: R7070-18, 17307017, F-HKU704/19, and 2122-7S04), the Health and Medical Research Fund (Fund number: HKM-15-M10), and the University of Hong Kong (University Research Committee and Norman & Cecilia Yip Foundation). We thank Profs. Vivian W.W. Yam and Quan Hao, and Drs. Menglong Hu and Yi Wang (Li Ka Shing Faculty of Medicine, The University of Hong Kong) for helpful comments and discussion. The crystal diffraction data were collected at SSRF, CAS. We thank the staff at the BL17U1 beamline of SSRF for their generous help.

Author affiliations: [a]Department of Chemistry, State Key Laboratory of Synthetic Chemistry, and CAS-HKU Joint Laboratory of Metallomics on Health and Environment, The University of Hong Kong, Hong Kong SAR, 999077, People's Republic of China; [b]Department of Chemistry and Molecular Engineering, East China Normal University, Shanghai, 200241, People's Republic of China; [c]Department of Microbiology, The University of Hong Kong, Hong Kong SAR, 999077, People's Republic of China; and [d]Applied Oral Sciences and Community Dental Care, Faculty of Dentistry, The University of Hong Kong, Hong Kong, 999077, People's Republic of China

1. J. Sun, H. Zhang, Y. H. Liu, Y. Feng, Towards understanding MCR-like colistin resistance. *Trends Microbiol.* **26**, 794–808 (2018).
2. L. L. Zhong *et al.*, High rates of human fecal carriage of *mcr-1*-positive multidrug-resistant Enterobacteriaceae emerge in China in association with successful plasmid families. *Clin. Infect. Dis.* **66**, 676–685 (2018).
3. J. S. Gunn, The *Salmonella* PmrAB regulon: Lipopolysaccharide modifications, antimicrobial peptide resistance and more. *Trends Microbiol.* **16**, 284–290 (2008).
4. C. R. MacNair *et al.*, Overcoming *mcr-1* mediated colistin resistance with colistin in combination with other antibiotics. *Nat. Commun.* **9**, 458 (2018).
5. S. J. Son, R. Huang, C. J. Squire, I. K. H. Leung, MCR-1: A promising target for structure-based design of inhibitors to tackle polymyxin resistance. *Drug Discov. Today* **24**, 206–216 (2019).
6. Y. Liu, S. Ding, J. Shen, K. Zhu, Nonribosomal antibacterial peptides that target multidrug-resistant bacteria. *Nat. Prod. Rep.* **36**, 573–592 (2019).
7. Y. Xu *et al.*, An evolutionarily conserved mechanism for intrinsic and transferable polymyxin resistance. *mBio* **9**, e02317 (2018).
8. R. Wang *et al.*, Bismuth antimicrobial drugs serve as broad-spectrum metallo-β-lactamase inhibitors. *Nat. Commun.* **9**, 439 (2018).
9. Y. Y. Liu *et al.*, Emergence of plasmid-mediated colistin resistance mechanism MCR-1 in animals and human beings in China: A microbiological and molecular biological study. *Lancet Infect. Dis.* **16**, 161–168 (2016).
10. B. van Loo *et al.*, An efficient, multiply promiscuous hydrolase in the alkaline phosphatase superfamily. *Proc. Natl. Acad. Sci. U.S.A.* **107**, 2740–2745 (2010).
11. P. Hinchliffe *et al.*, Insights into the mechanistic basis of plasmid-mediated colistin resistance from crystal structures of the catalytic domain of MCR-1. *Sci. Rep.* **7**, 39392 (2017).
12. V. Stojanoski *et al.*, Structure of the catalytic domain of the colistin resistance enzyme MCR-1. *BMC Biol.* **14**, 81 (2016).
13. G. Ma, Y. Zhu, Z. Yu, A. Ahmad, H. Zhang, High resolution crystal structure of the catalytic domain of MCR-1. *Sci. Rep.* **6**, 39540 (2016).
14. M. Hu *et al.*, Crystal structure of *Escherichia coli* originated MCR-1, a phosphoethanolamine transferase for colistin resistance. *Sci. Rep.* **6**, 38793 (2016).
15. L. Falgenhauer *et al.*; RESET consortium, Colistin resistance gene *mcr-1* in extended-spectrum β-lactamase-producing and carbapenemase-producing Gram-negative bacteria in Germany. *Lancet Infect. Dis.* **16**, 282–283 (2016).
16. S. J. Baker, D. J. Payne, R. Rappuoli, E. De Gregorio, Technologies to address antimicrobial resistance. *Proc. Natl. Acad. Sci. U.S.A.* **115**, 12887–12895 (2018).
17. L. Czaplewski *et al.*, Alternatives to antibiotics–A pipeline portfolio review. *Lancet Infect. Dis.* **16**, 239–251 (2016).
18. L. Ejim *et al.*, Combinations of antibiotics and nonantibiotic drugs enhance antimicrobial efficacy. *Nat. Chem. Biol.* **7**, 348–350 (2011).
19. M. Tyers, G. D. Wright, Drug combinations: A strategy to extend the life of antibiotics in the 21st century. *Nat. Rev. Microbiol.* **17**, 141–155 (2019).
20. K. Bush, P. A. Bradford, Interplay between β-lactamases and new β-lactamase inhibitors. *Nat. Rev. Microbiol.* **17**, 295–306 (2019).
21. J. R. Morones-Ramirez, J. A. Winkler, C. S. Spina, J. J. Collins, Silver enhances antibiotic activity against Gram-negative bacteria. *Sci. Transl. Med.* **5**, 190ra81 (2013).
22. C. H. Goss *et al.*, Gallium disrupts bacterial iron metabolism and has therapeutic effects in mice and humans with lung infections. *Sci. Transl. Med.* **10**, eaat7520 (2018).
23. M. B. Harbut *et al.*, Auranofin exerts broad-spectrum bactericidal activities by targeting thiol-redox homeostasis. *Proc. Natl. Acad. Sci. U.S.A.* **112**, 4453–4458 (2015).
24. J. A. Lemire, J. J. Harrison, R. J. Turner, Antimicrobial activity of metals: Mechanisms, molecular targets and applications. *Nat. Rev. Microbiol.* **11**, 371–384 (2013).
25. S. Reardon, Bacterial arms race revs up. *Nature* **521**, 402–403 (2015).
26. K. D. Mjos, C. Orvig, Metallodrugs in medicinal inorganic chemistry. *Chem. Rev.* **114**, 4540–4563 (2014).
27. H. Wang *et al.*, Deciphering molecular mechanism of silver by integrated omic approaches enables enhancing its antimicrobial efficacy in *E. coli*. *PLoS Biol.* **17**, e3000292 (2019).
28. H. Wang *et al.*, Antimicrobial silver targets glyceraldehyde-3-phosphate dehydrogenase in glycolysis of *E. coli*. *Chem. Sci. (Camb.)* **10**, 7193–7199 (2019).
29. European Committee on Antimicrobial Susceptibility Testing (EUCAST). Clinical breakpoints bacteria (v 12.0). https://www.eucast.org/clinical_breakpoints/. Accessed 5 March 2022.
30. I. Wiegand, K. Hilpert, R. E. Hancock, Agar and broth dilution methods to determine the minimal inhibitory concentration (MIC) of antimicrobial substances. *Nat. Protoc.* **3**, 163–175 (2008).
31. L. Zhang *et al.*, High-throughput synergy screening identifies microbial metabolites as combination agents for the treatment of fungal infections. *Proc. Natl. Acad. Sci. U.S.A.* **104**, 4606–4611 (2007).
32. S. R. Partridge *et al.*, Proposal for assignment of allele numbers for mobile colistin resistance (*mcr*) genes. *J. Antimicrob. Chemother.* **73**, 2625–2630 (2018).
33. H. Zhang *et al.*, Action and mechanism of the colistin resistance enzyme MCR-4. *Commun. Biol.* **2**, 36 (2019).
34. H. Li *et al.*, Molecular insights into functional differences between *mcr-3*- and *mcr-1*-mediated colistin resistance. *Antimicrob. Agents Chemother.* **62**, e00366-18 (2018).
35. A. Anandan *et al.*, Structure of a lipid A phosphoethanolamine transferase suggests how conformational changes govern substrate binding. *Proc. Natl. Acad. Sci. U.S.A.* **114**, 2218–2223 (2017).
36. H. Zhang, W. Wei, M. Huang, Z. Umar, Y. Feng, Definition of a family of nonmobile colistin resistance (NMCR-1) determinants suggests aquatic reservoirs for MCR-4. *Adv. Sci. (Weinh.)* **6**, 1900038 (2019).
37. F. Esposito *et al.*, Detection of colistin-resistant MCR-1-positive *Escherichia coli* by use of assays based on inhibition by EDTA and Zeta potential. *J. Clin. Microbiol.* **55**, 3454–3465 (2017).
38. J. P. Stratford *et al.*, Electrically induced bacterial membrane-potential dynamics correspond to cellular proliferation capacity. *Proc. Natl. Acad. Sci. U.S.A.* **116**, 9552–9557 (2019).
39. T. Wang, I. El Meouche, M. J. Dunlop, Bacterial persistence induced by salicylate via reactive oxygen species. *Sci. Rep.* **7**, 43839 (2017).
40. J. C. Dabrowiak, *Metals in Medicine* (John Wiley & Sons, ed. 2, 2017).

41. N. Yang *et al.*, Bismuth complexes inhibit the SARS coronavirus. *Angew. Chem. Int. Ed. Engl.* **46**, 6464–6468 (2007).
42. Y. Wang *et al.*, Integrative approach for the analysis of the proteome-wide response to bismuth drugs in *Helicobacter pylori*. *Chem. Sci. (Camb.)* **8**, 4626–4633 (2017).
43. D. Martinez Molina *et al.*, Monitoring drug target engagement in cells and tissues using the cellular thermal shift assay. *Science* **341**, 84–87 (2013).
44. R. Jafari *et al.*, The cellular thermal shift assay for evaluating drug target interactions in cells. *Nat. Protoc.* **9**, 2100–2122 (2014).
45. M. Barberon *et al.*, Monoubiquitin-dependent endocytosis of the iron-regulated transporter 1 (IRT1) transporter controls iron uptake in plants. *Proc. Natl. Acad. Sci. U.S.A.* **108**, E450–E458 (2011).
46. H. Öhrvik *et al.*, Ctr2 regulates biogenesis of a cleaved form of mammalian Ctr1 metal transporter lacking the copper- and cisplatin-binding ecto-domain. *Proc. Natl. Acad. Sci. U.S.A.* **110**, E4279–E4288 (2013).
47. Y. Hou *et al.*, Making the unconventional μ^2-P bridging binding mode more conventional in phosphinine complexes. *Chem. Sci. (Camb.)* **10**, 3168–3180 (2019).
48. P. J. Steel, C. J. Sumby, Coordination chemistry of di-2-pyridylmethane and related bridging ligands with silver(I), copper(II), palladium(II) and zinc(II). *Dalton Trans.* **2003**, 4505–4515 (2003).
49. B. Peters, N. Lichtenberger, E. Dornsiepen, S. Dehnen, Current advances in tin cluster chemistry. *Chem. Sci. (Camb.)* **11**, 16–26 (2019).
50. T. Zhou, S. Radaev, B. P. Rosen, D. L. Gatti, Structure of the ArsA ATPase: The catalytic subunit of a heavy metal resistance pump. *EMBO J.* **19**, 4838–4845 (2000).
51. R. Wang *et al.*, The global distribution and spread of the mobilized colistin resistance gene *mcr-1*. *Nat. Commun.* **9**, 1179 (2018).
52. Q. E. Yang *et al.*, Compensatory mutations modulate the competitiveness and dynamics of plasmid-mediated colistin resistance in *Escherichia coli* clones. *ISME J.* **14**, 861–865 (2020).
53. H. Sun *et al.*, Resensitizing carbapenem- and colistin-resistant bacteria to antibiotics using auranofin. *Nat. Commun.* **11**, 5263 (2020).
54. J. A. Al-Tawfiq, R. Laxminarayan, M. Mendelson, How should we respond to the emergence of plasmid-mediated colistin resistance in humans and animals? *Int. J. Infect. Dis.* **54**, 77–84 (2017).
55. M. Mohsin *et al.*, Description of the first *Escherichia coli* clinical isolate harboring the colistin resistance gene *mcr-1* from the Indian subcontinent. *Antimicrob. Agents Chemother.* **61**, e01945–e01916 (2016).
56. M. Hamel, J.-M. Rolain, S. A. Baron, The history of colistin resistance mechanisms in bacteria: Progress and challenges. *Microorganisms* **9**, 442 (2021).
57. L. Cao, X. Li, Y. Xu, J. Shen, Prevalence and molecular characteristics of *mcr-1* colistin resistance in *Escherichia coli*: Isolates of clinical infection from a Chinese University Hospital. *Infect. Drug Resist.* **11**, 1597–1603 (2018).
58. H.-M. Huang, P. Bellotti, F. Glorius, Transition metal-catalysed allylic functionalization reactions involving radicals. *Chem. Soc. Rev.* **49**, 6186–6197 (2020).